Highly anisotropic mechanical and optical properties of 2D layered As_2S_3 membranes

Šiškins, Makars; Lee, Martin; Alijani, Farbod; Van Blankenstein, Mark R.; Davidovikj, Dejan; Van Der Zant, Herre S.J.; Steeneken, Peter G.

DOI
10.1021/acsnano.9b06161

Publication date
2019

Document Version
Final published version

Published in
ACS Nano

ACS NANO

Cite This: ACS Nano 2019, 13, 10845−10851

www.acsnano.org

ARTICLE

Highly Anisotropic Mechanical and Optical Properties of 2D Layered As_2S_3 Membranes

Makars Šiškins,*,† Martin Lee,† Farbod Alijani,‡ Mark R. van Blankenstein,† Dejan Davidovikj,† Herre S. J. van der Zant,† and Peter G. Steeneken*,†,‡

†Kavli Institute of Nanoscience, Delft University of Technology, Lorentzweg 1, 2628 CJ Delft, The Netherlands

‡Department of Precision and Microsystems Engineering, Delft University of Technology, Mekelweg 2, 2628 CD Delft, The Netherlands

Supporting Information

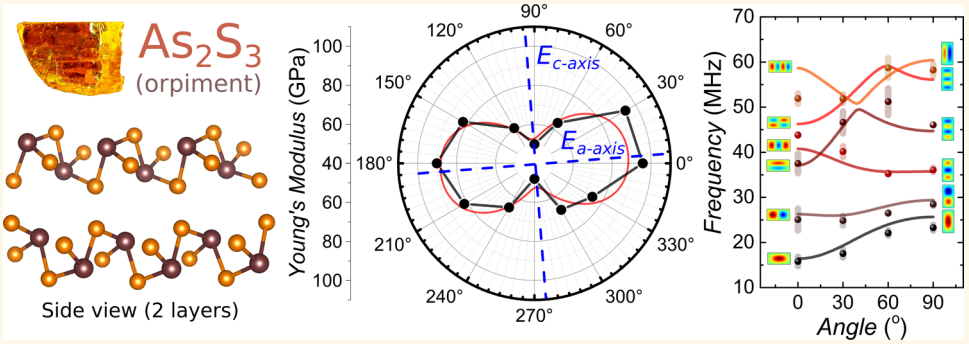

ABSTRACT: **Two-dimensional (2D) materials with strong in-plane anisotropy are of interest for enabling orientation-dependent, frequency-tunable, optomechanical devices. However, black phosphorus (bP), the 2D material with the largest anisotropy to date, is unstable as it degrades in air. In this work we show that As_2S_3 is an interesting alternative, with a similar anisotropy to bP, while at the same time having a much higher chemical stability. We probe the mechanical and optical anisotropy in As_2S_3 by three distinct angular-resolved experimental methods: Raman spectroscopy, atomic force microscopy (AFM), and resonance frequency analysis. Using a dedicated angle-resolved AFM force-deflection method, an in-plane anisotropy factor of $\frac{E_a}{E_c} = 1.7$ is found in the Young's modulus of As_2S_3 with $E_{a\text{-axis}} = 79.1 \pm 10.1$ GPa and $E_{c\text{-axis}} = 47.2 \pm 7.9$ GPa. The high mechanical anisotropy is also shown to cause up to 65% difference in the resonance frequency, depending on crystal orientation and aspect ratio of membranes.**

KEYWORDS: *mechanical anisotropy, 2D materials, arsenic trisulfide (As_2S_3), Raman spectroscopy, multimode resonances, nanoelectromechanical systems (NEMS)*

After the first exfoliation and characterization of graphene in 2004,[1] 2D crystals have attracted much interest as suspended membranes in mechanical systems due to their unprecedented high elastic moduli and strength.[2−5] Although resonators of many 2D materials, such as graphene and MoS_2, have been widely studied,[5−8] there are only a few 2D crystals known that exhibit large in-plane anisotropy.[9−14] Black phosphorus (bP) shows the largest known anisotropy in Young's modulus among 2D materials[15,16] with a ratio of $\frac{E_b}{E_a} = 2$ along the in-plane axes (b and a). However, few-layer bP is stable in air for only several minutes,[17] which severely affects its mechanical properties after oxidation[18] and complicates its application and integration into complex nanoelectromechanical systems (NEMS).

Here, we discuss the exfoliation of As_2S_3 including in its monolayer form and the fabrication of suspended membranes of this material. Although As_2S_3 has been studied and applied in its bulk and amorphous form, it has not received much attention in its ultrathin exfoliated form. The anisotropy in the Raman spectrum of As_2S_3 is compared to the mechanical anisotropy in its static deflection probed by atomic force microscopy (AFM) and in its dynamic deflection probed by a change in the resonance frequency of mechanical modes. We show that thin layers of As_2S_3 have a mechanical anisotropy comparable to that of black phosphorus, while their stability against degradation in ambient air facilitates integration and

Received: August 5, 2019
Accepted: August 15, 2019
Published: August 15, 2019

DOI: 10.1021/acsnano.9b06161
ACS Nano 2019, 13, 10845−10851

study of few-layer As_2S_3 resonators in complex mechanical devices. In addition to that, the material has perspectives to become an important member of the class of 2D materials due to a unique combination of properties: As_2S_3 is known to transmit infrared well,[19] has an optical indirect band gap of ~2.6 eV,[20,21] shows photoconductivity,[22,23] and has a large acousto-optical figure of merit.[24] This combination of properties makes it of interest for fundamental studies of anisotropic phenomena in 2D materials, but can also enable new types of applications such as acousto-optic modulators.[25]

RESULTS AND DISCUSSION

Structure and Characterization. Arsenic trisulfide, also known as orpiment,[26] is a naturally occurring layered crystal. The unit cell of the As_2S_3 lattice consists of two layers inverted through a symmetry center located in a van der Waals gap (Figure 1b). From the crystallographical point of view, a unit

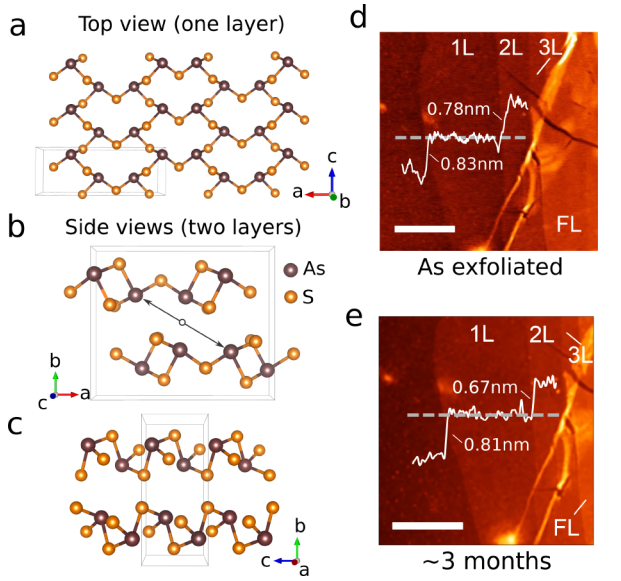

Figure 1. Crystal structure and atomic force microscopy (AFM) images of As_2S_3. (a) Crystal lattice of a single-layer As_2S_3. Projection along the *b*-axis. Gray box indicates a single unit cell. (b) Projection along the *a*-axis. Inversion center is indicated. (c) Projection along the *c*-axis. (d, e) AFM images of a nanometer-thin exfoliated layer of As_2S_3 on SiO_2/Si as fabricated and after ~3 months in air. Scale bars: 1 μm.

cell of arsenic trisulfide is defined by 20 atoms (10 atoms for a monolayer)[21] compared to two for graphene, three for MoS_2, and eight for black phosphorus, which makes it one of the most structurally complex 2D materials known. Natural As_2S_3 crystals are of a high purity (see Supporting Information (SI) 1), have low interlayer binding energy,[21,27] and have an exfoliation energy comparable to graphite.[20] These properties enable the use of conventional methods for exfoliation and transfer of flakes[28,29] when additional safety precautions are applied due to the toxicity of the material.[30,31] Natural crystals of As_2S_3 can be well exfoliated, as indicated by the tapping mode AFM measurements in Figure 1d, which show flakes as thin as 0.83 nm with consecutive step heights ranging from 0.7 to 0.8 nm. The monolayer thickness is expected to be a half of the unit cell along the *b*-axis, $t_{As_2S_3}$ = 0.5 × 0.96 nm = 0.48 nm.[26] Since the step height observed in AFM is less than twice the layer thickness, we conclude that we have exfoliated a monolayer of As_2S_3. A similar 40−60% difference between the measured AFM step height and expected thickness of a single layer has been also observed in AFM studies of other 2D materials and might be related to intercalation effects.[33] As shown in the AFM image in Figure 1e, the thickness of the As_2S_3 monolayer remains virtually unchanged after three months in air under ambient light. The multilayer flakes of As_2S_3, which were exfoliated from the same crystal as the monolayer, are stable for hours at low or ambient light conditions (see SI 1), such that it is likely that no degradation occurs in the absence of light. This stability is an important advantage over other strongly anisotropic 2D materials such as black phosphorus that decompose rapidly in air,[17] as can be seen in AFM measurements.[34] The stability in ambient conditions of As_2S_3 can be attributed to its low solubility in water[32,35] and low oxidation rate in air in the absence of excessive exposure to light.[36,37]

We fabricated a number of samples with flake thicknesses, *t*, varying from 0.8 to 129 nm. Flakes were transferred on top of a prepatterned Si/SiO_2 chip with 12 rectangular cavities. Each subsequent rectangle is rotated by a 30° angle with respect to the previous one and has a length of the longest side, *b*, considerably larger than its width, *a*. We estimate the orientation of the optical axes of each flake using polarized light microscopy,[10] thus taking advantage of the transcendent in-plane birefringence of the crystal: $\Delta n_{As_2S_3}$ measures ~0.35 around visible frequencies,[38] which is ~1.4× higher than of black phosphorus and ~10× that of ReS_2.[12] This allows us to coarse-align the optical axes of the flakes to one of the cavities (see SI 2). A flake transferred on top of this prepatterned array of cavities forms a star-shaped mechanical resonator, such that the stiffness of each membrane in the structure is dominated by the mechanical properties along the shorter side of the rectangle.

Polarization-Dependent Raman Spectroscopy. We have studied the anisotropy of arsenic trisulfide in detail by polarization-dependent Raman spectroscopy[39] at λ = 488, 514, and 632 nm of a laser excitation (see SI 7). At λ = 632 nm the measured Raman spectrum shows at least eight vibrational modes: seven symmetric (A_1) and one asymmetric (B_2) (Figure 2a) with respect to rotations around the principal axis, corresponding to a C_{2v}^7 point group symmetry of a single As_2S_3 layer.[40,41] These could be related to a C_{2h} point group symmetry of the bulk crystal through a correlation table.[40−43] The intensity of Raman modes depends on the linear polarization angle of incident light in a backscattering Raman setup. As shown in Figure 2d−f, A_1 (154 and 202 cm^{-1}), Raman modes have the largest intensity when the light polarization is aligned along the *a*-axis, while the A_1 (309 cm^{-1}) mode has the maximum intensity along the *c*-axis.[40−43] We explain this behavior using group theory and Raman tensor calculations, assuming Placzek approximation (see SI 3), which produces a good fit to the measured data (Figure 2d−f). The frequency of Raman phonons did not depend on the measured flake thickness, although the intensity of the signal decreased accordingly (Figure 2c). We used this polarization-dependent Raman mode to determine the exact crystalline orientation for flakes of thicknesses down to 8 nm. At a smaller number of layers (*e.g.*, 2 nm of thickness) the signal of the Si from the substrate starts to dominate the spectra. We have also performed photodegradation tests by analyzing the Raman spectrum of the 354−358 cm^{-1} modes under a set of laser

DOI: 10.1021/acsnano.9b06161
ACS Nano 2019, 13, 10845−10851

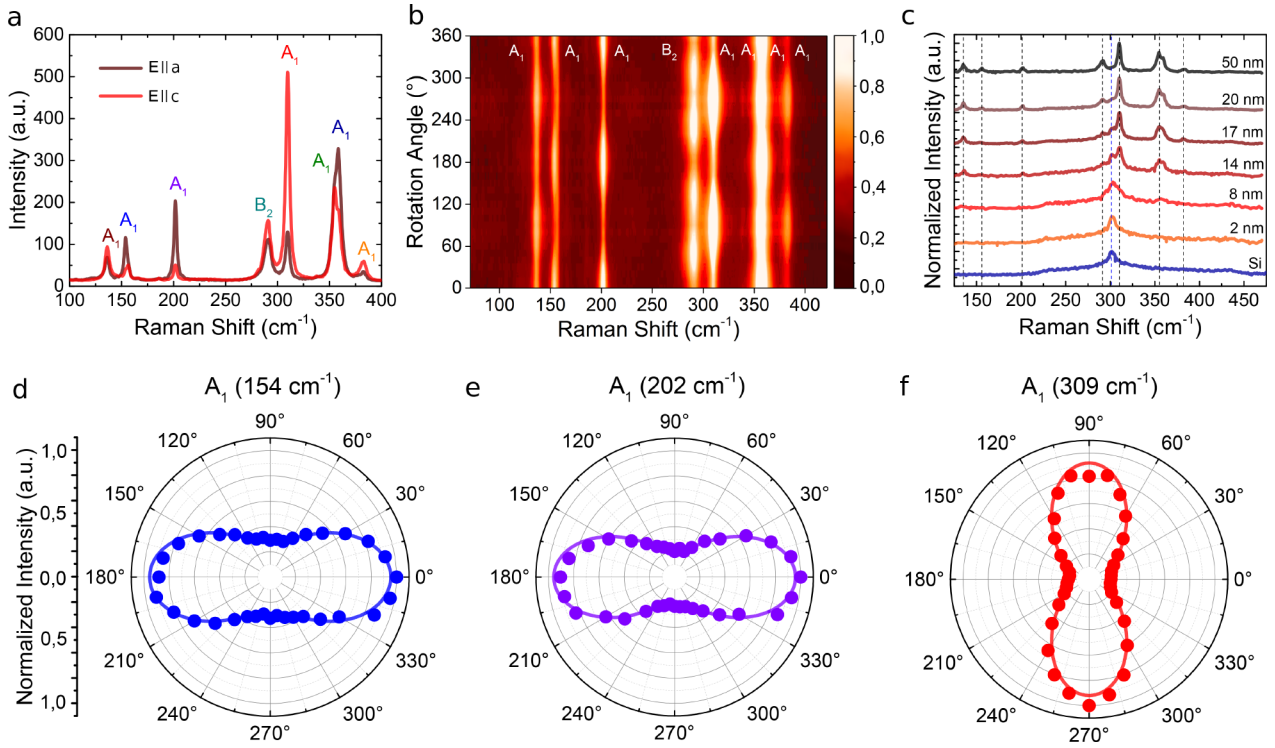

Figure 2. (a) Raman spectra of a bulk As_2S_3 crystal (thickness, $t \approx 50$ nm) for a polarization of incident red laser light ($\lambda = 632$ nm) along two crystalline axes (*a* and *c*). (b) Polarization-dependent Raman intensity spectra obtained by sample rotation with normal incident light (along the *b*-axis of a crystal). (c) Thickness-dependent Raman spectra under $\lambda = 632$ nm excitation. (d–f) Polarization dependence for three Raman-active modes. Vibrational modes in a, b, and d–f are labeled in accordance to previous works[40−45] on As_2S_3.

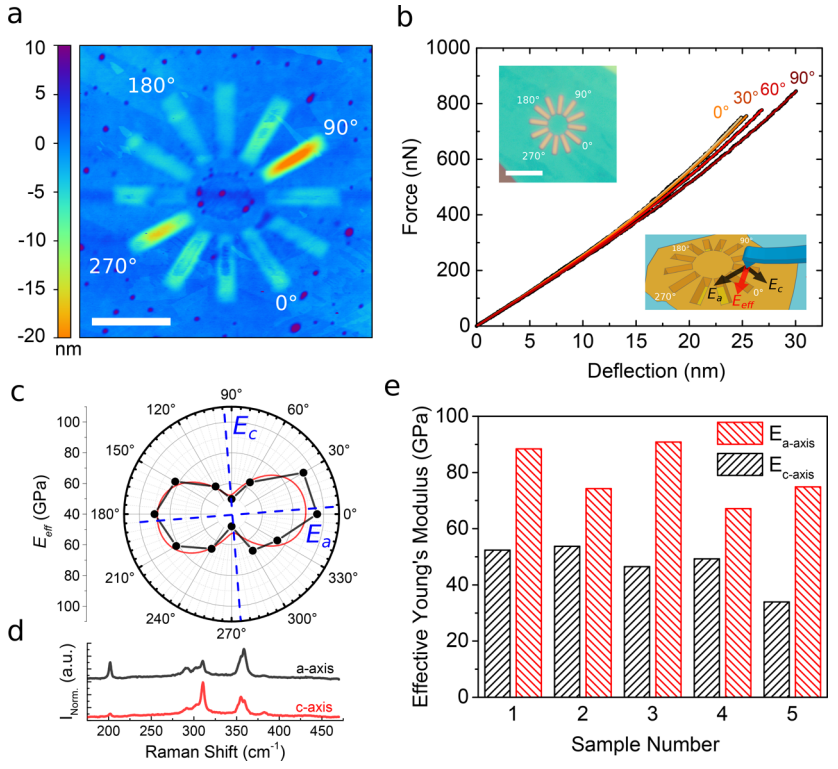

Figure 3. Detailed angle-resolved study of the Young's modulus of As_2S_3. (a) Tapping mode AFM image of the sample. Scale bar: 4 μm. (b) Typical force−deflection curve obtained at different angles of a rectangular cavity with respect to crystalline axes. Top inset: Optical image of the sample. Scale bar: 8 μm. Bottom inset: Principle of the measurement. (c) Angle-resolved effective Young's modulus of the membrane. Red line is a fit to eq 2. Young's moduli for in-plane crystalline directions (E_a and E_c) are indicated. (d) Raman spectra along each axis. (e) Effective Young's modulus along *a* and *c* crystalline axes measured for the best five samples of various thickness (from 9 to 25 nm).

DOI: 10.1021/acsnano.9b06161
ACS Nano 2019, 13, 10845−10851

powers. Although As_2S_3 is known to transmit infrared well,[19] approaching the band gap of the material (~2.6 eV[21,46]) with excessive light can convert the crystal to its amorphous state,[47] thus locally destroying the crystallinity of the flake (see SI 1). Taking this into account, we further used flakes of thicknesses t > 8 nm and a corresponding low power of the incident laser light to minimize damage to the suspended As_2S_3 membranes.

Anisotropy in the Static Mechanical Properties. The strong asymmetry of the crystalline structure of As_2S_3 along the a- and c-axes (Figure 1b,c) is also expected to cause a large anisotropy in the Young's modulus of the material.[48] We have studied the mechanical anisotropy in the Young's modulus as a function of angle by AFM using the star-shaped configuration shown in Figure 3a. With an AFM tip of calibrated stiffness we indent the As_2S_3 membranes suspended over star-shaped trenches and record the force−deflection curve at the center of each of the 12 membranes of the same flake. The high aspect ratio of the rectangular membranes, $b \gg a$ is chosen such that the slope of the force−deflection curve is dominated by the effective Young's modulus, E_{eff}, along the shortest side of the rectangle. As shown in Figure 3b, a difference in deflection, δ, was achieved for an equal force applied, F. Assuming a point force deflection at the center of the cavity, we obtain the following equation for the force−distance relation of the rectangular membrane (see SI 4):

$$F = \frac{E_{eff} t^3}{12\alpha(1-\nu^2)a^2}\delta + C_2 N_0 \delta + \frac{c_0}{(1-\nu^2)^{0.85}}\frac{E_{eff} t}{a^2}\delta^3 \quad (1)$$

where $\alpha(a, b)$, $C_2(a, b)$, and $c_0(a, b)$ are geometry-dependent factors and N_0 is the intrinsic pretension. Using Poisson's ratio $\nu^2 = 0.094$,[49,50] we fit eq 1 to the data and extract effective Young's moduli along the set of angles to the crystalline axes. We take into account measured thickness variations as determined by AFM, which are found to be at most one to two single layers (as seen in Figure 3a), to extract correct values of E_{eff}. Figure 3c shows the characteristic dumbbell shape of angle-resolved effective Young's moduli, which is a typical example of mechanical anisotropy in layered materials.[16] We also measure Raman spectra along the hard and soft axis of the crystal to connect the observed anisotropy in mechanical properties to the crystalline orientation (Figure 3d). The dependence of E_{eff} on the rotation angle, θ, in a particular direction is defined from Hooke's law, taking into the account E_a, E_c, and an effective shear, G_{eff} (see SI 5):[16]

$$E_{eff}(\theta) = \frac{1}{\frac{1}{E_a}\cos^4\theta + \left(\frac{1}{G_{eff}} - \frac{2\nu}{E_a}\right)\sin^2\theta\cos^2\theta + \frac{1}{E_c}\sin^4\theta} \quad (2)$$

From the fits of eq 2 to the data in Figure 3c,e we obtain E_a = 79.1 ± 10.1 GPa, E_c = 47.2 ± 7.9 GPa, and G_{eff} = 28.0 ± 2.5 GPa, so that the ratio of the mechanical anisotropy is $\frac{E_a}{E_c} \approx 1.7$ (Figure 3e). These values are also consistent with additional measurements done on synthetically grown As_2S_3 showing that effect of possible defects and stacking faults on mechanical anisotropy in natural As_2S_3 crystals is insignificant (see SI 6).

Dynamic Mechanical Properties. When As_2S_3 is suspended over a rectangular hole made in a Si/SiO_2 substrate, it forms a resonator. We use the light intensity modulation by the motion of the membrane to measure the resonance frequencies in a laser interferometer. A schematic of the setup is shown in Figure 4a. Here, the modulated blue diode laser is used to optothermally drive the As_2S_3 membrane and the red

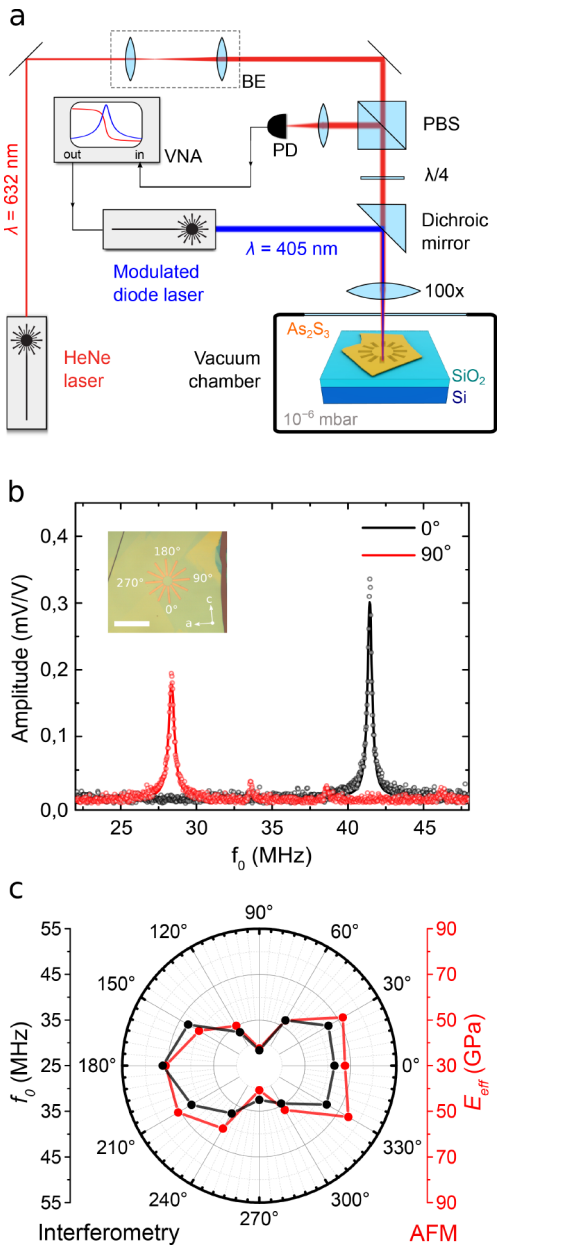

Figure 4. Measurement setup and measured angle-resolved frequency response of the device. (a) Schematic of the measurement setup. (b) Angle-dependent frequency response of rectangular resonators rotated by 90° with respect to the *a*-axis. (c) Comparison of anisotropic response observed in motion (laser interferometry, black) and statics (AFM force-indention, red).

laser to read out its motion.[51] This allowed us to observe a significant shift in the resonance frequency of the fundamental mode, $f_0(\theta)$, at θ = 90° to the hard axis (a-axis) of the crystal (Figure 4b). We were also able to resolve the natural mode frequency as a function of crystalline orientation of a membrane and compare it to the effective Young's modulus extracted for the same flake with the force−deflection AFM measurements. As shown in Figure 4c, the ratio of anisotropy measures $\frac{E_a}{E_c} = \left(\frac{f_0(0°)}{f_0(90°)}\right)^2 = 2.0 \pm 0.3$ in the dynamic experi-

DOI: 10.1021/acsnano.9b06161
ACS Nano 2019, 13, 10845−10851

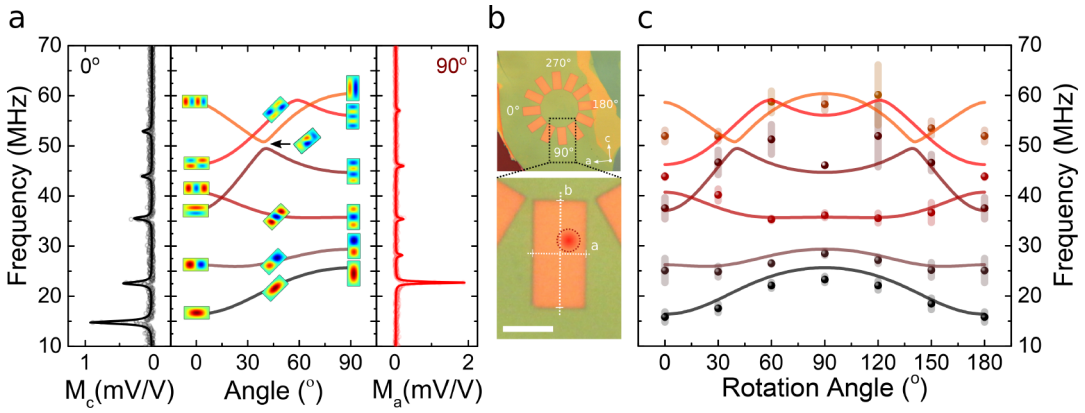

Figure 5. Change in resonance frequency of vibrational modes of an As_2S_3 plate. (a) Finite element model (FEM) for the first six modes of a resonator compared to the measured magnitude (M_c, M_a) of resonance peaks at 0° and 90° rotation of the rectangular membrane with respect to the *c*-axis of the crystal. (b) Optical image of a device with orientation and scales indicated. Dimensions are a = 5 μm and b = 10 μm. Scale bar: 5 μm. Both blue and red lasers are focused at the position indicated by the red circle in the lower panel. (c) Vibrational mode frequencies with corresponding errors compared to the FEM model.

ment, which is comparable to $\frac{E_a}{E_c} = 1.8 \pm 0.1$ found from the static deflection of the same flake. This confirms the significant effect of anisotropy in the Young's modulus on the mechanical response of the membranes.

We further investigated the evolution of higher modes of thick rectangular As_2S_3 resonators as a function of the angle to the crystalline axis. We transferred a 129 ± 3 nm thick flake, as measured by tapping mode AFM, over a set of rectangular cavities with a b:a = 2:1 side ratio (Figure 5b). This aspect ratio results in mode crossings[52] at certain angles, θ, and a more complex frequency dependence on angle for higher modes.[53] In Figure 5a,c the solid lines show the results of a finite element method (FEM) model obtained using the COMSOL Multiphysics package of the first six modes of a clamped As_2S_3 plate resonator. The model matches experimental data well (Figure 5a and c) for the first four modes. Note that no fitting parameters were used, with only the thickness measured from AFM and elastic constants[48] of As_2S_3 added as an input to the FEM simulations. For higher modes we observe a discrepancy between the measured position of the resonance peak and the model, which could be due to a larger sensitivity of higher modes to perturbations and imperfections of the system.[51] We show six modes obtained from FEM simulation together with five experimentally detected modes in Figure 5c to emphasize that the highest measured mode could not be precisely identified but is likely to be related to either the fifth or sixth mode of the resonator. Interestingly, as can be seen in Figure 5a, an avoided crossing is expected when the long side of the rectangular membrane with b/a = 2 aspect ratio makes an angle of 40° with respect to the *c*-axis of the crystal. This unique feature could be potentially used in further studies of strong intrinsic coupling and internal resonances between modes in rectangular resonators of different ratio of sides.[52]

CONCLUSIONS

In conclusion, we combined optical and mechanical characterization techniques to obtain a comprehensive picture of the in-plane anisotropy in arsenic trisulfide. Using polarization-dependent Raman spectroscopy and force−deflection AFM in a star-shaped geometry of rectangular cavities, we systematically characterized the mechanical anisotropy in a few layers of this van der Waals crystal and relate that to its crystalline structure and orientation. We showed quantitatively that the anisotropy in the Young's modulus of As_2S_3 is close to that of black phosphorus, which is currently known to have the largest in-plane $\frac{E_a}{E_b}$ ratio among 2D crystals.[15] We also demonstrated that this results in a large orientation-specific change in the resonance frequency of higher vibrational modes in As_2S_3 resonators. These mechanical properties make As_2S_3 an interesting alternative to black phosphorus for applications in flexible strain-dependent optoelectronical devices,[20] while stability in air makes it a promising material for further integration into optomechanical nanodevices as well as for research of anisotropic nonlinear mechanics in the 2D limit. We also believe that, due to its high flexibility[48−50] and pronounced optoelectronic properties,[38,46] As_2S_3 has perspectives to find applications in atomically thin optical waveplates[12] and to become an interesting candidate material for polarization-sensitive flexible photoconductors[22,23] and acousto-optic modulators.[24]

METHODS

Sample Fabrication. A prepatterning on a Si/SiO_2 (285 nm) chip was implemented by reactive ion etching (RIE), and edges were examined to be well-defined by scanning electron microscopy (SEM) and AFM. Flakes of As_2S_3 were exfoliated from a matrix crystal mined in Senduchen, Sakha Republic, Russia. Thin flakes of As_2S_3 were transferred on a prepatterned chip by an all-dry viscoelastic stamping method.[28]

Raman Spectroscopy. Raman spectroscopy studies were performed on a Horiba Scientific LabRAM HR at an excitation of λ_{red} = 632 nm, λ_{green} = 514 nm, and λ_{blue} = 488 nm in a backscattering geometry in parallel-polarized configuration, ($e_i \parallel e_s$) with a 360° rotational sample stage. All measurements were performed away from the suspended region.

Atomic Force Microscopy. AFM scans and inspections were performed in tapping mode on a Bruker Dimension FastScan AFM. Cantilevers were chosen to have a tip radius of ∼7−10 nm, as confirmed by SEM imaging. Using thermal and solid surface deflection calibration we estimated the spring constant, k, for each cantilever. We use cantilevers with spring constants of k = 30−40 N/m for thicker flakes (>12 nm) and k = 8−9 N/m for thinner ones (<12 nm). Each data point on the polar diagram in Figure 3a is an averaged value from fitting three to five force−deflection curves obtained at the same position.

DOI: 10.1021/acsnano.9b06161
ACS Nano 2019, 13, 10845−10851

Laser Interferometry. The sample is mounted on a motorized *xy* nanopositioning stage inside a vacuum chamber with optical access. A modulated diode laser (λ = 405 nm) was used to excite the membrane optothermally and drive it into motion. An interferometric displacement detection is then obtained by focusing a He−Ne laser beam (λ = 632 nm) on the suspended membrane while recording the interfering reflections from the membrane and the Si substrate underneath using a photodiode. Laser spot size is on the order of ∼1 μm. The photodiode signal is processed by a vector network analyzer. The pressure inside the vacuum chamber is kept stable at $\sim 1 \times 10^{-6}$ mbar.

ASSOCIATED CONTENT

Supporting Information

The Supporting Information is available free of charge on the ACS Publications website at DOI: 10.1021/acsnano.9b06161.

Stability and photodegradation of As_2S_3, polarized light microscopy, polarization-dependent Raman spectroscopy, derivation of force−deflection equation for a rectangular plate with pretension, fit of the effective Young's modulus, mechanical properties of the synthetic lab-grown As_2S_3, wavelength- and polarization-dependent Raman spectroscopy of synthetic and natural As_2S_3 crystals (PDF)

AUTHOR INFORMATION

Corresponding Authors

*E-mail: m.siskins-1@tudelft.nl.

*E-mail: P.G.Steeneken@tudelft.nl.

ORCID

Makars Šiškins: 0000-0003-4295-2221

Dejan Davidovikj: 0000-0002-6593-458X

Notes

The authors declare no competing financial interest.

ACKNOWLEDGMENTS

This project has received funding from the European Union's Horizon 2020 Research and Innovation Program (grant no. 785219). F.A. acknowledges financial support from European Research Council (ERC) (grant no. 802093).

REFERENCES

(1) Novoselov, K. S.; Geim, A. K.; Morozov, S. V.; Jiang, D.; Zhang, Y.; Dubonos, S. V.; Grigorieva, I. V.; Firsov, A. A. Electric Field Effect in Atomically Thin Carbon Films. *Science* **2004**, *306*, 666−669.

(2) Lee, C.; Wei, X.; Kysar, J. W.; Hone, J. Measurement of the Elastic Properties and Intrinsic Strength of Monolayer Graphene. *Science* **2008**, *321*, 385−388.

(3) Androulidakis, C.; Zhang, K.; Robertson, M.; Tawfick, S. Tailoring the Mechanical Properties of 2D Materials and Heterostructures. *2D Mater.* **2018**, *5*, No. 032005.

(4) Akinwande, D.; Brennan, C. J.; Bunch, J. S.; Egberts, P.; Felts, J. R.; Gao, H.; Huang, R.; Kim, J.-S.; Li, T.; Li, Y.; Liechti, K. M.; Lu, N.; Park, H. S.; Reed, E. J.; Wang, P.; Yakobson, B. I.; Zhang, T.; Zhang, Y.-W.; Zhou, Y.; Zhu, Y. A Review on Mechanics and Mechanical Properties of 2D Materials − Graphene and Beyond. *Extreme Mech. Lett.* **2017**, *13*, 42−77.

(5) Bunch, J. S.; van der Zande, A. M.; Verbridge, S. S.; Frank, I. W.; Tanenbaum, D. M.; Parpia, J. M.; Craighead, H. G.; McEuen, P. L. Electromechanical Resonators from Graphene Sheets. *Science* **2007**, *315*, 490−493.

(6) Chen, C.; Rosenblatt, S.; Bolotin, K. I.; Kalb, W.; Kim, P.; Kymissis, I.; Stormer, H. L.; Heinz, T. F.; Hone, J. Performance of Monolayer Graphene Nanomechanical Resonators with Electrical Readout. *Nat. Nanotechnol.* **2009**, *4*, 861.

(7) Castellanos-Gomez, A.; Singh, V.; van der Zant, H. S. J.; Steele, G. A. Mechanics of Freely-Suspended Ultrathin Layered Materials. *Ann. Phys. (Berlin, Ger.)* **2015**, *527*, 27−44.

(8) Davidovikj, D.; Alijani, F.; Cartamil-Bueno, S. J.; van der Zant, H. S. J.; Amabili, M.; Steeneken, P. G. Nonlinear Dynamic Characterization of Two-Dimensional Materials. *Nat. Commun.* **2017**, *8*, 1253.

(9) Sa, B.; Chen, J.; Yang, X.; Yang, H.; Zheng, J.; Xu, C.; Li, J.; Wu, B.; Zhan, H. Elastic Anisotropy and Optic Isotropy in Black Phosphorene/Transition-Metal Trisulfide van der Waals Heterostructures. *ACS Omega* **2019**, *4*, 4101−4108.

(10) Shen, W.; Hu, C.; Tao, J.; Liu, J.; Fan, S.; Wei, Y.; An, C.; Chen, J.; Wu, S.; Li, Y.; Liu, J.; Zhang, D.; Sun, L.; Hu, X. Resolving the Optical Anisotropy of Low-Symmetry 2D Materials. *Nanoscale* **2018**, *10*, 8329−8337.

(11) Tian, H.; Tice, J.; Fei, R.; Tran, V.; Yan, X.; Yang, L.; Wang, H. Low-Symmetry Two-Dimensional Materials for Electronic and Photonic Applications. *Nano Today* **2016**, *11*, 763−777.

(12) Yang, H.; Jussila, H.; Autere, A.; Komsa, H.-P.; Ye, G.; Chen, X.; Hasan, T.; Sun, Z. Optical Waveplates Based on Birefringence of Anisotropic Two-Dimensional Layered Materials. *ACS Photonics* **2017**, *4*, 3023−3030.

(13) Yang, S.; Hu, C.; Wu, M.; Shen, W.; Tongay, S.; Wu, K.; Wei, B.; Sun, Z.; Jiang, C.; Huang, L.; Wang, Z. In-Plane Optical Anisotropy and Linear Dichroism in Low-Symmetry Layered TlSe. *ACS Nano* **2018**, *12*, 8798−8807.

(14) Zhou, X.; Hu, X.; Jin, B.; Yu, J.; Liu, K.; Li, H.; Zhai, T. Highly Anisotropic GeSe Nanosheets for Phototransistors with Ultrahigh Photoresponsivity. *Adv. Sci.* **2018**, *5*, 1800478.

(15) Tao, J.; Shen, W.; Wu, S.; Liu, L.; Feng, Z.; Wang, C.; Hu, C.; Yao, P.; Zhang, H.; Pang, W.; Duan, X.; Liu, J.; Zhou, C.; Zhang, D. Mechanical and Electrical Anisotropy of Few-Layer Black Phosphorus. *ACS Nano* **2015**, *9*, 11362−11370.

(16) Wei, Q.; Peng, X. Superior Mechanical Flexibility of Phosphorene and Few-Layer Black Phosphorus. *Appl. Phys. Lett.* **2014**, *104*, 251915.

(17) Castellanos-Gomez, A.; Vicarelli, L.; Prada, E.; Island, J. O.; Narasimha-Acharya, K. L.; Blanter, S. I.; Groenendijk, D. J.; Buscema, M.; Steele, G. A.; Alvarez, J. V.; Zandber- gen, H. W.; Palacios, J. J.; van der Zant, H. S. J. Isolation and Characterization of Few-Layer Black Phosphorus. *2D Mater.* **2014**, *1*, No. 025001.

(18) Moreno-Moreno, M.; Lopez-Polin, G.; Castellanos-Gomez, A.; Gomez-Navarro, C.; Gomez-Herrero, J. Environmental Effects in Mechanical Properties of Few-Layer Black Phosphorus. *2D Mater.* **2016**, *3*, No. 031007.

(19) Frerichs, R. New Optical Glasses with Good Transparency in the Infrared. *J. Opt. Soc. Am.* **1953**, *43*, 1153.

(20) Miao, N.; Zhou, J.; Sa, B.; Xu, B.; Sun, Z. Few-Layer Arsenic Trichalcogenides: Emerging Two-Dimensional Semiconductors with Tunable Indirect-Direct Band-Gaps. *J. Alloys Compd.* **2017**, *699*, 554−560.

(21) Debbichi, L.; Kim, H.; Björkman, T.; Eriksson, O.; Lebègue, S. First-Principles Investigation of Two-Dimensional Trichalcogenide and Sesquichalcogenide Monolayers. *Phys. Rev. B: Condens. Matter Mater. Phys.* **2016**, *93*, 245307.

(22) Blossey, D. F. Iodine Quenching of the Surface Photoresponse of Crystalline As_2S_3. *Chem. Phys. Lett.* **1974**, *25*, 593−595.

(23) Blossey, D. F.; Zallen, R. Surface and Bulk Photoresponse of Crystalline As_2S_3. *Phys. Rev. B* **1974**, *9*, 4306−4313.

(24) Rouvaen, J. M.; Bridoux, E.; Moriamez, M.; Torguet, R. Acoustic Anharmonic Properties of Arsenic Trisulfide Glass. *Appl. Phys. Lett.* **1974**, *25*, 97−99.

(25) Khan, M.; Mahmoud, A.; Cai, L.; Mahmoud, M.; Mukherjee, T.; Bain, J. A.; Piazza, G. Acousto-Optic Modulator based on the Integration of Arsenic Trisulfide Photonic Com- ponents with Lithium Niobate Surface Acoustic Waves. *Proceedings of 2019 Conference on Lasers and Electro-Optics (CLEO)* **2019**, *8750211*, 1−2.

(26) Mullen, D. J. E.; Nowacki, W. Refinement of the Crystal Structures of Realgar, AsS and Orpiment, As_2S_3. *Z. Kristallogr. Cryst. Mater.* **1972**, *136*, 48−65.
(27) Gibbs, G. V.; Wallace, A. F.; Zallen, R.; Downs, R. T.; Ross, N. L.; Cox, D. F.; Rosso, K. M. Bond Paths and van der Waals Interactions in Orpiment, As_2S_3. *J. Phys. Chem. A* **2010**, *114*, 6550−6557.
(28) Castellanos-Gomez, A.; Buscema, M.; Molenaar, R.; Singh, V.; Janssen, L.; van der Zant, H. S. J.; Steele, G. A. Deterministic Transfer of Two-Dimensional Materials by All-Dry Viscoelastic Stamping. *2D Mater.* **2014**, *1*, No. 011002.
(29) Pizzocchero, F.; Gammelgaard, L.; Jessen, B. S.; Caridad, J. M.; Wang, L.; Hone, J.; Bøggild, P.; Booth, T. J. The Hot Pick-Up Technique for Batch Assembly of van der Waals Heterostructures. *Nat. Commun.* **2016**, *7*, 11894.
(30) Ozakin, E.; Can, R.; Kaya, F.; Acar, N.; Cevik, A. A. Arsenic Poisoning Due to the Intake of Orpiment. *J. Clin. Toxicol.* **2014**, *04* (3), 176.
(31) Buchanan, J. A.; Eberhardt, A.; Tebb, Z. D.; Heard, K.; Wendlandt, R. F.; Kosnett, M. J. Massive Human Ingestion of Orpiment (Arsenic Trisulfide). *J. Emerg. Med.* **2013**, *44*, 367−372.
(32) Liu, J.; Lu, Y.; Wu, Q.; Goyer, R. A.; Waalkes, M. P. Mineral Arsenicals in Traditional Medicines: Orpiment, Realgar, and Arsenolite. *J. Pharmacol. Exp. Ther.* **2008**, *326*, 363−368.
(33) Shearer, C. J.; Slattery, A. D.; Stapleton, A. J.; Shapter, J. G.; Gibson, C. T. Accurate Thickness Measurement of Graphene. *Nanotechnology* **2016**, *27*, 125704.
(34) Wood, J. D.; Wells, S. A.; Jariwala, D.; Chen, K.-S.; Cho, E.; Sangwan, V. K.; Liu, X.; Lauhon, L. J.; Marks, T. J.; Hersam, M. C. Effective Passivation of Exfoliated Black Phosphorus Transistors Against Ambient Degradation. *Nano Lett.* **2014**, *14*, 6964−6970.
(35) Fowler, B. A.; Chou, C.-H. S. J.; Jones, R. L.; Chen, C.-J. In *Handbook on the Toxicology of Metals*, 3rd ed.; Nordberg, G. F., Fowler, B. A., Nordberg, M., Friberg, L. T., Eds.; Elsevier: San Diego, 2007; pp 367−406.
(36) Allen, P. J.; Johnson, B. R.; Riley, B. J. Photo-Oxidation of Thermally Evaporated As_2S_3 Thin Films. *J. Optoelectron. Adv. Mater.* **2005**, *7*, 3281−3291.
(37) Lengke, M. F.; Tempel, R. N. Reaction Rates of Natural Orpiment Oxidation at 25 to 40°C and pH 6.8 to 8.2 and Comparison with Amorphous As_2S_3 Oxidation. *Geochim. Cosmochim. Acta* **2002**, *66*, 3281−3291.
(38) Zallen, R.; Blossey, D. F. In *Optical and Electrical Properties*; Lee, P. A., Ed.; Springer: Dordrecht, 1976; pp 231−272.
(39) Zhu, W.; Liang, L.; Roberts, R. H.; Lin, J.-F.; Akinwande, D. Anisotropic Electron-Phonon Interactions in Angle-Resolved Raman Study of Strained Black Phosphorus. *ACS Nano* **2018**, *12*, 12512−12522.
(40) Zallen, R.; Slade, M. L.; Ward, A. T. Lattice Vibrations and Interlayer Interactions in Crystalline As_2S_3 and As_2Se_3. *Phys. Rev. B* **1971**, *3*, 4257−4273.
(41) Razzetti, C.; Lottici, P. Polarization Analysis of the Raman Spectrum of As_2S_3 Crystals. *Solid State Commun.* **1979**, *29*, 361−364.
(42) DeFonzo, A. P.; Tauc, J. Network Dynamics of 3:2 Coordinated Compounds. *Phys. Rev. B: Condens. Matter Mater. Phys.* **1978**, *18*, 6957−6972.
(43) Mamedov, S.; Drichko, N. Characterization of 2D As_2S_3 Crystal by Raman Spectroscopy. *MRS Adv.* **2018**, *3*, 385−390.
(44) Kobliska, R. J.; Solin, S. A. Temperature Dependence of the Raman Spectrum and the Depolarization Spectrum of Amorphous As_2S_3. *Phys. Rev. B* **1973**, *8*, 756−768.
(45) Klein, P. B.; Taylor, P. C.; Treacy, D. J. Two-Phonon Vibrational Spectra of As_2S_3. I. Crystalline Phase. *Phys. Rev. B* **1977**, *16*, 4501−4510.
(46) Drews, R.; Emerald, R.; Slade, M.; Zallen, R. Interband Spectra of As_2S_3 and As_2Se_3 Crystals and Glasses. *Solid State Commun.* **1972**, *10*, 293−296.
(47) Frumar, M.; Firth, A.; Owen, A. Optically Induced Crystal-to-Amorphous-State Transition in As_2S_3. *J. Non-Cryst. Solids* **1995**, *192*−*193*, 447−450.
(48) McNeil, L. E.; Grimsditch, M. Elastic Constants of As_2S_3. *Phys. Rev. B: Condens. Matter Mater. Phys.* **1991**, *44*, 4174−4177.
(49) Glaze, F.; Blackburn, D.; Osmalov, J.; Hubbard, D.; Black, M. Properties of Arsenic Sulfide Glass. *J. Res. Natl. Bur. Stand.* **1957**, *59*, 83.
(50) Greaves, G. N.; Greer, A. L.; Lakes, R. S.; Rouxel, T. Poisson's Ratio and Modern Materials. *Nat. Mater.* **2011**, *10*, 823−837.
(51) Davidovikj, D.; Slim, J. J.; Cartamil-Bueno, S. J.; van der Zant, H. S. J.; Steeneken, P. G.; Venstra, W. J. Visualizing the Motion of Graphene Nanodrums. *Nano Lett.* **2016**, *16*, 2768−2773.
(52) Chang, S. I.; Bajaj, A. K.; Krousgrill, C. M. Non-linear Vibrations and Chaos in Harmonically Excited Rectangular Plates with One-to-One Internal Resonance. *Nonlinear Dyn.* **1993**, *4*, 433−460.
(53) Wang, Z.; Feng, P. X.-L. Design of Black Phosphorus 2D Nanomechanical Resonators by Exploiting the Intrinsic Mechanical Anisotropy. *2D Mater.* **2015**, *2*, No. 021001.

DOI: 10.1021/acsnano.9b06161
ACS Nano 2019, 13, 10845−10851